

Influence of Support Material of PtSnNiGa/C Electrocatalysts for Ethanol Oxidation

Deise M. Santos^{a,b}, Giordano T. Paganoto^a, Maria A. R. Queiroz^a, Marco C. C. Guimarães^c, Josimar Ribeiro^{a,*}

^aUniversidade Federal do Espírito Santo, Centro de Ciências Exatas, Departamento de Química, Av. Fernando Ferrari, 514, CEP29075-910, Vitória, Espírito Santo, Brazil.

^bInstituto Federal do Espírito Santo, Diretoria de Pós-graduação, Av. Rio Branco, 50, CEP29056-255, Vitória, Espírito Santo, Brazil.

^cUniversidade Federal do Espírito Santo, Centro de Ciências da Saúde, Departamento de Morfologia, CEP29049-999, Maruípe, Vitória, Espírito Santo, Brasil.

Article history: Received: 06 February 2017; revised: 25 May 2017; accepted: 30 May 2017. Available online: 25 June 2017.
DOI: <http://dx.doi.org/10.17807/orbital.v9i3.949>

Abstract: Ethanol is a promising alternative source for fuel cells due to its low toxicity and high power density. However, the cleavage of the C-C bond, CO poisoning, and low electrocatalyst stability are still considered crucial issues. To overcome this limitation, binary, ternary and quaternary electrocatalysts have been investigated along with new carbon supports. This paper presents a physicochemical and electrochemical investigation of quaternary PtSnNiGa/C electrocatalysts supported on Vulcan XC72 and Printex-L6 carbons and also a carbon produced by natural gas pyrolysis in an Argon plasma torch (Black Plasma). The electrochemical characterization was performed through cyclic voltammetry, chronoamperometry, chronopotentiometry and electrochemical impedance spectroscopy in the presence of ethanol 1.0 mol L⁻¹. Energy dispersive X-ray spectroscopy, X-ray diffraction, Raman spectroscopy and transmission electron microscopy were also carried out for physicochemical characterization. The electrochemical results show that the quaternary electrocatalysts supported on Vulcan XC72 and Printex-L6 carbons display a high current normalized by Pt mass and are more stable than the electrocatalyst supported on Black Plasma. In addition, the quaternary electrocatalysts with reduced Pt loading display better electrocatalytic activity towards the EOR compared to high Pt loading electrocatalysts.

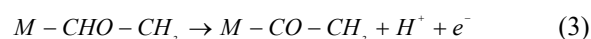
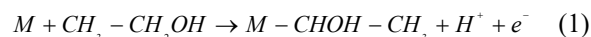
Keywords: ethanol oxidation reaction; gallium; proton exchange membrane fuel cells; quaternary electrocatalysts

1. INTRODUCTION

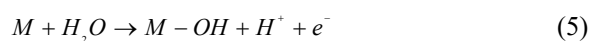
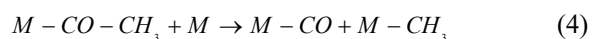
Polymer electrolyte membrane fuel cells (PEMFCs) is a device that converts the energy present in chemical bonds to electrical energy and heat through electrochemical reactions, they are considered promising long-term power sources [1,2]. Along with PEMFC technology development, low molecular alcohols, such as methanol and ethanol, have been tested as alternative fuels to hydrogen due to their liquid form, storage capacity, high power density and their ability to be directly fed to the anode [3]. Compared to methanol, ethanol is less toxic and has a theoretical energy density of 8 kWh kg⁻¹ whereas the value for methanol is 6 kWh kg⁻¹ [4]. In addition, ethanol is a renewable energy source

that can be produced by agricultural bioprocesses [5].

The Pt-based electrocatalysts are best known for dissociative adsorption of small organic molecules at low temperatures, including ethanol [6]. A widely-accepted mechanism for the ethanol oxidation reaction (EOR) comprises the sequence of steps represented by the following equations (*M* is the metal active site) [7]:



*Corresponding author. E-mail: josimar.ribeiro@ufes.br



Ethanol can also be absorbed directly by M-OH species to form acetate by means of a 4e⁻ mechanism as follows [8]:



An efficient electrocatalyst should facilitate the dehydrogenation process (Eqs.(1)-(3)), C-C bond cleavage (Eq.(4)) and CO_{ads} oxidation (Eq. (6)). In addition, water activation (Eq.(5)) at a low potential is important for the CO_{ads} and C2 species oxidation [7,8]. However, the Pt-based electrocatalytic activity is limited, considering the C-C bond cleavage, and two carbon species have been mainly identified due to incomplete ethanol oxidation. Moreover, pure Pt electrocatalysts are highly susceptible to poisoning by species, such as CO and CH_x, during the EOR [9].

Thus far, PtSn/C and PtRu/C have been considered some of the most efficient electrocatalysts for EOR [10]. The addition of Sn induce an extension of the Pt-Pt distance, which promotes a dissociative adsorption of ethanol molecules in a lower potential [11]. Moreover, SnO_x species increases water activation at lower potentials than pure Pt, which decreases CO poisoning [12]. Almeida et al. [13] showed that Ni addition to PtSn/C diminishes the potential at which ethanol and CO oxidation occur due to electronic effects; however, the ternary electrocatalyst was not able to cleave the C-C bond.

Bonesi et al. [14] reported that the partial substitution of Sn by Ni atoms leads to a variation in the Pt d-band occupancy, which is related to electrocatalytic activity improvement. In another study, Bonesi et al. [9] showed that the presence of Ni oxide species, such as NiO, Ni(OH)₂, and NiOOH, contribute to the oxidation of CO and CH₃CO at lower potentials.

According to Hogarth et al. [15] the PtGa/C electrocatalysts, supported on Vulcan XC72R carbon, present a promotional effect towards the methanol oxidation reaction compared to any of the Pt/C, PtPd/C, PtOs/C and PtIr/C electrocatalysts. Recently, Kumar et al. [16]

showed that alloyed Pt-Ga supported on graphene has potential use as an electrocatalyst for methanol oxidation. The presence of Ga downshifts Pt d-band centre compared to pure Pt, leading to a weaker interaction between CO_{ads} species and Pt active site [16,17]. Also, it has been reported that a small Ga addition to Pt catalyst would reduce EOR onset potential, although, as soon as 30% weight of Ga is added to Pt, passive amorphous gallium oxides is extended [18].

In this sense, the addition of metals in the platinum catalysts allows the so-called bifunctional mechanism and the electronic interaction between the metals. Better activity of polymetallic electrocatalysts can be explained by the synergistic effect between those metals, increasing the number of structural defects, solid solutions or roughness, beyond that, Pt dependence is reduced [12,13].

Besides metallic composition, the stability of carbon support is a quit challenge for PEMFCs. New carbon materials have been tested as supports in order to improve catalytic activity, stability and corrosion resistance [19-22]. Features, such as the abundance of defective sites, the presence of organic groups on the surface and a large number of pores, make Vulcan XC72 carbon the most common material used as a support for electrocatalyst synthesis [21]. However, other sorts of carbon-based materials, such as carbon nanotubes [23], nanofibers [24], and graphene sheets [25], are being studied as supports for platinum-based electrocatalysts.

In a recent study, a carbon black produced by natural gas pyrolysis in Argon plasma (Black Plasma) was investigated as a support for a Pt/C electrocatalyst [26]. The EOR current values for Pt/C supported on Black Plasma were higher than the current values for similar electrocatalysts supported on Vulcan XC72 carbon. Another alternative to commercial carbon support is the Printex L6, a high-surface-area carbon black used for generation of H₂O₂ in alkaline medium by oxygen reduction reaction (ORR) [27,28]. Despite its potential, very scarce information about Black Plasma and Printex L6 carbons have been found in the literature. Wherefore, verifying a support influence of new materials on polymetallic electrocatalytic activity for EOR is necessary.

2. MATERIAL AND METHODS

The first procedure consists of a treatment of the carbon supports by placing 2 g of carbon support in boiling water at 100 °C for 30 min and then rising with water at room temperature. After water withdrawn, carbon supports were placed in a boiling solution of 2.0 mol L⁻¹ H₂SO₄ (Sigma-Aldrich) for 30 min. The warm solution was vacuum filtered, and the residual carbon was dried in an oven at 100 °C and calcined at 400 °C for 1 h in an air atmosphere. This procedure was performed on the Vulcan XC72, Printex L6 and Black Plasma carbons.

The electrocatalysts were prepared by thermal decomposition of polymeric precursors method (DPP) [29,30]. The precursors (metal resin) for each metal were prepared by mixing citric acid (Merck) in ethylene glycol (Merck) between 60 °C - 65 °C. After complete dissolution of the citric acid in ethylene glycol, a 0.2 mol L⁻¹ solution of metal ion in 50 mL of isopropanol (Merck) was slowly added to the mixture to produce the resin, providing a molar ratio of 1:4:16 of metal, citric acid, and ethylene glycol, respectively. After complete addition of the metal precursor solution, the temperature was increased until 80 °C - 85 °C for esterification. The resins for Pt, Sn, Ni and Ga were synthesized using H₂PtCl₆.6H₂O (Sigma-Aldrich), SnCl₂ (Sigma-Aldrich), Ni(NO₃)₂.6H₂O (Sigma-Aldrich) and Ga(NO₃)₃ (Sigma-Aldrich) as metal precursors. An ICP OES (PerkinElmer, model Optima 7300V) was used for quantification of Pt, Sn, Ni and Ga at respective metal resins. The optimized parameters as well as the limit of Detection (LOD), the Limit of Quantification (LOQ) and the metal concentration are presented in Table S1 of [supplementary material](#).

The synthesis of Pt₅₀Sn₂₀Ni₂₅Ga₅/C electrocatalysts supported on Vulcan XC72, Printex-L6 and Black Plasma consisted of preparing 50 mg of electrocatalyst, in which 60 wt% (30 mg) corresponds to the treated carbon support and 40 wt% (20 mg) corresponds to the total amount of metal. The required mass of each metal was calculated from their respective molar fractions using Eq. (8).

$$m_i = x_i MM_i \frac{m}{\sum_i x_i MM_i} \quad (8)$$

where m_i , MM_i and x_i are the metal mass, molar weight and mole fractions of each metal,

respectively, and m is the total metal loading of the electrocatalyst. The carbon amount and resin necessary quantities were placed in a glass vial along with 1 mL of ethanol. The resulting mixture was ultrasonicated in a Thornton T14 model bath for 30 min for the dispersion homogeneous of the material. After that, the solvent was completely evaporated in an oven at 80 °C for overnight period, followed by annealing at 350 °C in an oven for 3 hours in an air atmosphere. The Pt₅₀Sn₂₀Ni₂₅Ga₅/C_{XC72}, Pt₅₀Sn₂₀Ni₂₅Ga₅/C_{L6} and Pt₅₀Sn₂₀Ni₂₅Ga₅/C_{Plasma} nominal compositions were obtained after the annealing step.

Physicochemical characterizations

The X-ray diffraction (XRD) was performed on a Bruker D8 diffractometer with K_αCu radiation ($\lambda = 1.5406 \text{ \AA}$), with a scan in 2θ from 10° to 90° and step rate of 0.01° min⁻¹. The crystallite size (D) was estimated using the Scherrer equation [31].

$$D = \frac{K\lambda}{\beta \cos \theta_\beta} \quad (9)$$

where K is the shape factor (0.9 for spherical crystallites), λ is the wavelength, β is the diffraction full width at the half-maximum intensity ($FWHM$) and θ_β is the angle at maximum intensity and the wavelength. The morphology and dispersion of metal particles in the electrocatalyst carbon support were analysed by transmission electron microscopy (TEM) using an electron microscope JEOL/JEM-1400 model. In addition, the Raman spectra of the Printex L6 support in the range of 0 to 3000 cm⁻¹ was obtained using a confocal microscope WITEC 300R Alpha with a 533 nm monochromatic beam. Scanning electron microscopy coupled with energy-dispersive X-ray spectroscopy (SEM-EDS) was performed using a scanning electron microscope from Carl Zeiss EVO 10 model to obtain the experimental composition of the electrocatalysts.

Electrochemical characterization

The electrochemical characterization was performed using a 0.5 mol L⁻¹ H₂SO₄ (Sigma-Aldrich) as the supporting electrolyte (SE). The

counter electrode was a graphite electrode with a geometric area of 4 cm² and a silver/silver chloride electrode [Ag/AgCl, KCl_{sat}] was used as the reference electrode. The working electrode was prepared by depositing 100 μL of an ink, consisting of 1 mg of catalyst dispersed in 5 μL of 5%Nafion® (Sigma-aldrich) and 95 μL of ethanol, on a graphite electrode with a geometric area of 0.16 cm² previously polished with alumina (0.3 μm).

The electrocatalytic activity of the materials was evaluated by cyclic voltammetry (CV) in the potential range of -0.15 V to 1.0 V vs [Ag/AgCl, KCl_{sat}] in SE, in the presence and absence of 1.0 mol L⁻¹ ethanol. The chronoamperometry was performed in a 1.0 mol L⁻¹ solution of ethanol in SE at a constant potential of 0.2 V vs [Ag/AgCl, KCl_{sat}] for 120 min. The electrochemical impedance spectroscopy (EIS) was carried out in a 1.0 mol L⁻¹ solution of ethanol in SE at 0.2 V vs [Ag/AgCl, KCl_{sat}] in a frequency range of 100 kHz to 10 mHz in the single sine

mode with an amplitude of 5 mV p/p. Chronopotentiometry was carried out in a 1.0 mol L⁻¹ solution of ethanol in SE at a constant current density of 3 mA cm⁻² for 15 h to evaluate the effects of CO poisoning. The stability of the electrocatalysts was evaluated by 1000 cycles in SE in the potential range of -0.15 V to 1.0 V vs [Ag/AgCl, KCl_{sat}]. All the electrochemical tests were performed in a Metrohm potentiostat/galvanostat Autolab 128N model.

3. RESULTS AND DISCUSSION

The EDS analysis of Pt₅₀Sn₂₀Ni₂₅Ga₅/C (hereafter called the experimental composition) electrocatalysts supported on Vulcan XC72, Printex L6 and Black Plasma carbons (Table 1) indicates that the experimental composition is close to nominal composition. The weight variation of 17.3% for Pt₄₁Sn₂₄Ni₂₃Ga₁₂/C_{Plasma} is probably due to the oxidation of carbon to CO₂ during the annealing step.

Table 1. Experimental mass and EDS results obtained for the PtSnNiGa electrocatalyst supported on Vulcan XC72, Printex–L6 and Black Plasma carbons prepared by the DPP process.

Electrocatalyst/nominal composition	Electrocatalyst/experimental composition	Theoretical mass/mg	Experimental mass/mg	Variation/ %
Pt ₅₀ Sn ₂₀ Ni ₂₅ Ga ₅ /C _{XC72}	Pt ₄₅ Sn ₂₂ Ni ₂₁ Ga ₁₂ /C _{XC72}	50	49.2	1.6
Pt ₅₀ Sn ₂₀ Ni ₂₅ Ga ₅ /C _{L6}	Pt ₄₃ Sn ₂₄ Ni ₂₂ Ga ₁₁ /C _{L6}	50	47.4	5.2
Pt ₅₀ Sn ₂₀ Ni ₂₅ Ga ₅ /C _{Plasma}	Pt ₄₁ Sn ₂₄ Ni ₂₃ Ga ₁₂ /C _{Plasma}	30	24.8	17.3

The Raman spectra of the Printex L6 carbon (Figure 1) shows the well-known peaks of the D band at 1350 cm⁻¹ and G band at 1580 cm⁻¹ and the 2D resonance peak [32]. The intensity of the G band and the ratio I (D)/(G) = 1.1 suggesting the presence of carbon with sp² hybridization [33]. This same characteristic has already been observed for Vulcan XC72 and Black Plasma carbon in our previous work [26]. The high material graphitisation contributes to electrical conductivity, reducing the electrode resistance and protecting the carbon support from being oxidized [19].

The XRD pattern of the PtSnNiGa/C supported on the Vulcan XC72, Printex-L6 and Black Plasma carbons (Figure 2) shows the well-known face-centered cubic (fcc) crystalline Pt for all electrocatalysts. The Pt peaks position for all

electrocatalysts are shifted to lower 2θ values compared to the XRD pattern of pure Pt (PDF 35-1360) [34] indicating that the lattice parameters obtained for the three electrocatalysts are expanded regarding the pure Pt lattice parameter (*a* = 3.923 Å). This expansion is probably due to the incorporation of other metals into the Pt face-centred cubic structure. The presence of Sn (atomic radius = 151 pm) [35] atoms in crystalline Pt (atomic radius= 139 pm) [35] structure leads to a displacement of the XRD peak positions to lower 2θ values than pure Pt XRD, which leads to larger lattice parameters [13].

Considering the different crystalline structures for Pt and Sn (face-centred cubic for Pt and tetragonal for Sn), and the difference in electronegativity between these metals (2.2 Pauling units for Pt and 1.96 for Sn) [36], the formation of a new phase (Pt₃Sn) is expected

and has been already reported in the literature. However, the existence of a solid solution is not discarded due to the low atomic radius difference (151 pm for Sn and 139 pm for Pt). The presence of Ni atoms (atomic radius = 125 pm) [36] and Ga atoms (atomic radius = 122 pm) [36] shifts the XRD peak positions to higher 2θ values than those of pure Pt XRD, leading to a lattice parameter contraction [9,13], but this effect was not observed. The formation of crystalline oxides was not verified by XRD.

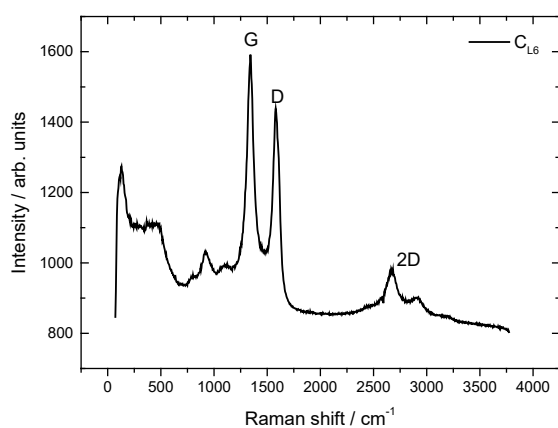


Figure 1. C_{L6} carbon black Raman spectra at 532nm wavelength.

However, this hypothesis should not be dismissed because of the high oxygen content in the composition obtained by EDS (7.2 to 13.7 % wt.). Oxides (SnO_x , PtO_x , NiO_x , Ga_xO_y) might be amorphous or less than the amount detectable by XRD. The crystallite size was estimated using Eq.(9), and the results are shown in Table 2. The $Pt_{45}Sn_{22}Ni_{21}Ga_{12}/C_{XC72}$ electrocatalyst showed a smaller crystallite size (5.5 – 2.1 nm) compared to $Pt_{43}Sn_{24}Ni_{22}Ga_{11}/C_{L6}$ (7.0 – 4.1 nm) and $Pt_{41}Sn_{24}Ni_{23}Ga_{12}/C_{Plasma}$ (7.8 – 4.4 nm) electrocatalysts.

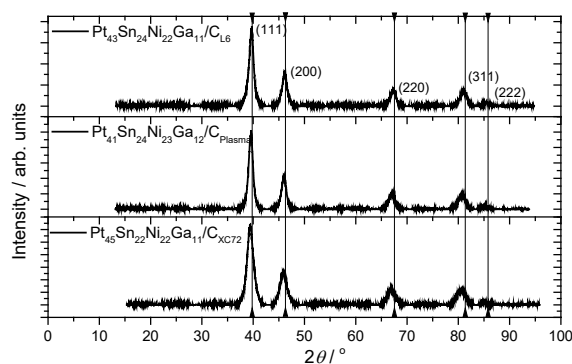


Figure 2. XRD Patterns for quaternary PtSnNiGa/C electrocatalysts supported on carbon Vulcan XC72, Printex-L6 and Black Plasma.

Table 2. XRD results for the PtSnNiGa electrocatalyst supported on Vulcan XC72, Printex–L6 and Black Plasma carbons prepared by the DPP process.

Electrocatalysts	a / Å	V / Å ³	D / nm				
			111	200	220	311	222
$Pt_{45}Sn_{22}Ni_{21}Ga_{12}/C_{XC72}$	3.959	62.07 ± 0.01	5.5	4.9	4.8	4.6	2.1
$Pt_{41}Sn_{24}Ni_{23}Ga_{12}/C_{Plasma}$	3.946	61.03 ± 0.01	7.8	7.2	6.4	5.9	4.4
$Pt_{43}Sn_{24}Ni_{22}Ga_{11}/C_{L6}$	3.937	61.46 ± 0.01	7.0	7.1	6.0	5.3	4.7

A homogeneous distribution of $Pt_{45}Sn_{22}Ni_{21}Ga_{12}/C_{XC72}$ nanoparticles over Vulcan XC72 carbon was confirmed from TEM micrographs (Figure 3A) wherein there was a formation of nanoparticle clusters for $Pt_{43}Sn_{24}Ni_{22}Ga_{11}/C_{L6}$ (Figure 3B) and $Pt_{41}Sn_{24}Ni_{23}Ga_{12}/C_{Plasma}$ (Figure 3C). This configures a disadvantage of both carbons because can lead to a worse catalytic activity due to the loss of metallic surface area. Particle sizes obtained for all the electrocatalysts are consistent with values already reported for Pt electrocatalysts [37,38] and corroborate with the results observed in the XRD data.

The cyclic voltammetry of the PtSnNiGa/C electrocatalysts in SE are presented in Figure 4A

(The carbon supports cyclic voltammetry in SE are presented on Figure S1 of [Supplementary Material](#)). For the $Pt_{45}Sn_{20}Ni_{25}Ga_{12}/C_{XC72}$ electrocatalyst the desorption/adsorption peaks in the hydrogen oxidation region (–0.10 V – 0.2 V vs [Ag/AgCl, KCl_{sat}]) are not well defined regarding pure Pt. As can be seen, the $Pt_{45}Sn_{20}Ni_{25}Ga_{12}/C_{XC72}$ electrocatalyst shows better charge densities compared to others electrocatalysts (it is perhaps due to higher Pt active sites availability). Meanwhile, for the $Pt_{41}Sn_{24}Ni_{23}Ga_{12}/C_{Plasma}$ and $Pt_{43}Sn_{24}Ni_{22}Ga_{11}/C_{L6}$ electrocatalysts, the desorption/adsorption peaks of hydrogen do not appear at all. This behaviour maybe a result of lower amounts of Pt active sites because of cluster formation in these electrocatalysts. This

conclusion is agreement with the TEM data (see Figure 3). Moreover, the presence of other metals and oxides, such as Sn, Ni, Ga, NiO_x, GaO_x and

SnO_x species maybe block the Pt active sites at low potentials as well [18, 27,39].

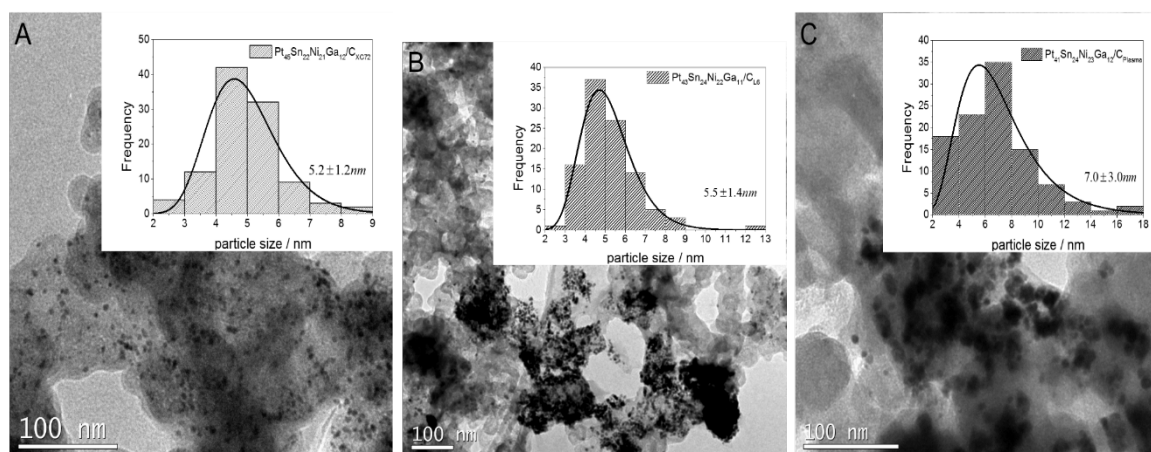


Figure 3. TEM images and histograms of particle sizes for the: (A) Pt₄₅Sn₂₀Ni₂₅Ga₁₂/C_{XC72}, (B) Pt₄₃Sn₂₄Ni₂₂Ga₁₁/C_{L6} and (C) Pt₄₁Sn₂₄Ni₂₃Ga₁₂/C_{Plasma}.

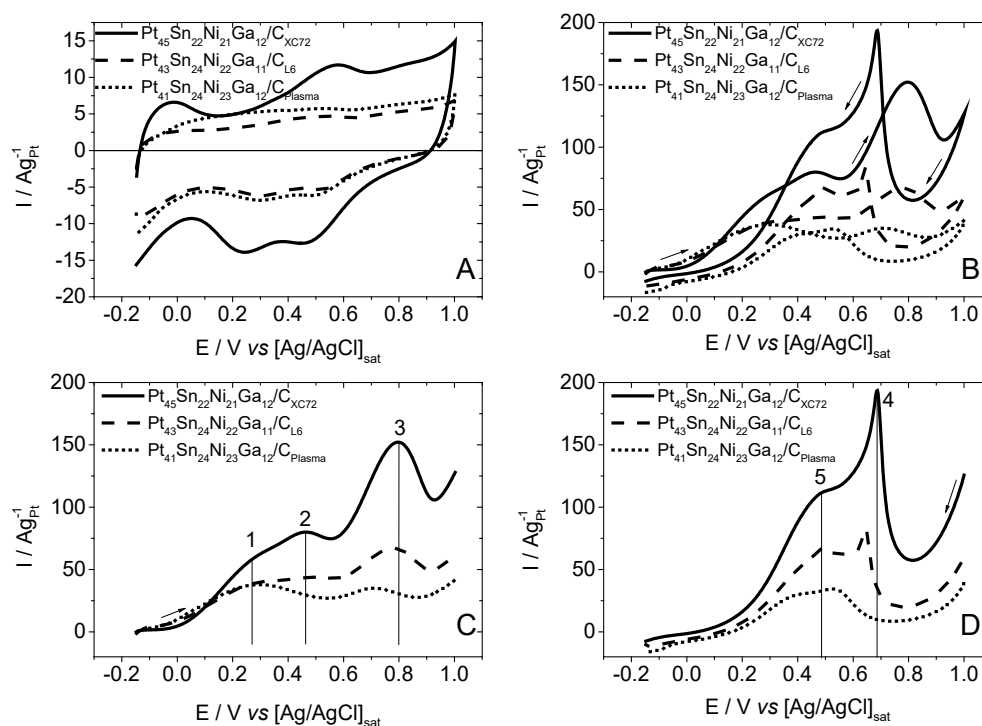


Figure 4. Cyclic voltammograms in (A) SE, (B) cyclic voltammograms in ethanol 1.0 mol L⁻¹, (C) positive-going potential scan in ethanol 1.0 mol L⁻¹ and (D) negative-going potential scan in ethanol 1.0 mol L⁻¹ of the PtSnNiGa/C electrocatalysts supported on Vulcan XC72, Printex-L6 and Black Plasma carbons. Scan rate of 20 mVs⁻¹.

The Electrochemical Active Surface Area (EASA) of pure Pt electrode could be estimated if the oxidation charge of a hydrogen monolayer in a polished Pt electrode is 210 μCcm⁻² [40,41]. Mathematically the EASA was calculated as follows:

$$EASA = \frac{Q_H}{0.21x[Pt]} \quad (10)$$

Wherein Q_H is the desorption hydrogen charge and [Pt] is the Pt concentration in gcm⁻². Despite of the electrocatalysts reported in this

study possess other metals, the Q_H charge could be estimated by integrating the area of hydrogen desorption region at $-0.15\text{ V} - 0.15\text{ V}$ vs [Ag/AgCl, KCl_{sat}], subtracting the double layer contribution charge [40,41]. (Unfortunately, this subtraction was impossible for the Pt₄₁Sn₂₄Ni₂₃Ga₁₂/Plasma electrocatalyst, thus, the EASA for this composition was not calculated). The EASA values are shown in Table 3.

The cyclic voltammograms in SE none normalized, normalized by electrode geometric area and EASA are presented on Figure S2A and Figure S2B and Figure S2C, respectively in the [Supplementary Material](#). The normalization by Pt loading can provide information about the influence of other metals on the electrocatalysts behaviour. One can see, the CV profile obtained for the PtSnNiGa/C electrocatalysts no change when the current was normalized by Pt loading, or current densities (mA cm^{-2}) or normalized by EASA. The results show that the normalization does not interfere in the interpretation of the data obtained in this investigation.

The cyclic voltammograms in 1 mol L⁻¹ ethanol in SE shown in the Figure 4B, 4C and 4D (The cyclic voltammograms in ethanol 1.0 mol L⁻¹ none normalized, normalized by electrode geometric area and normalized by EASA are presented on Figure S3A, Figure S3B and Figure S3C, respectively, in the [Supplementary Material](#)). For better viewing, Figure 4B is divided in positive going potential scan (Figure 4C) and negative going potential scan (Figure 4D). In Figure 4C, the current values in the region of adsorption/desorption of hydrogen are smaller when compared to Figure 4A due to adsorption of ethanol molecules on the electrode surface. The peaks (1), (2) and (3) in the positive-going potential scan, might be related to the acetaldehyde formation at lower overpotential ($< 0.6\text{ V}$ vs [Ag/AgCl, KCl_{sat}]) [42,43]. It can be noted that the Pt₄₁Sn₂₄Ni₂₃Ga₁₂/C_{Plasma} electrocatalyst presents the peaks (2) and (3) in lower overpotentials comparing to Pt₄₅Sn₂₀Ni₂₅Ga₁₂/C_{XC72} and Pt₄₃Sn₂₄Ni₂₃Ga₁₂/C_{L6}. The peak (1) in Pt₄₅Sn₂₀Ni₂₅Ga₁₂/C_{XC72} cyclic voltammetry might be related to water activation step which occurs at approximately 0.3 V vs [Ag/AgCl, KCl_{sat}] [42,43]. In the negative-going potential scan (Figure 4D); the Pt₄₅Sn₂₂Ni₂₁Ga₁₂/C_{XC72}, Pt₄₃Sn₂₄Ni₂₂Ga₁₁/C_{L6} presents peaks (4) and (5) which are related to the oxidation of ethanol, after which the by-products

remain on the reactivated surface of the Pt electrocatalyst [28,43].

Chronoamperometry is another key analysis for electrocatalytic activity and stability evaluation towards EOR. A high current value for ethanol oxidation is a crucial characteristic of a good electrocatalyst. The chronoamperometry of PtSnNiGa/C electrocatalysts in 1.0 mol L⁻¹ ethanol in SE solution recorded at a constant potential of 0.2 V vs [Ag / AgCl, KCl_{sat}] for 2 h (Figure 5A) (The i vs t curves of PtSnNiGa/C electrocatalysts none normalized and normalized by electrode geometric area and the EASA are shown in the Figure S4A, Figure S4B and Figure S4C, respectively, in the [Supplementary Material](#)) shows that in all curves there is a slight initial current drop followed by a slower decay. The rapid fall is well-known in the literature and is associated with the strong adsorption of species, such as CO, CH_x and C_xH_yO_z, on the active sites of the Pt, which can restrict the propagation of the oxidation mechanism [44-48]. At longer times, the current drop may be related to the instability of metal nanoparticles on the carbon support surface due to factors, such as crystallization, segregation of the metal and agglomeration, leading to lower current values [49,50]. The final current values (after 2 h) for Pt₄₅Sn₂₂Ni₂₁Ga₁₂/C_{XC72}, Pt₄₃Sn₂₄Ni₂₂Ga₁₁/C_{L6} and Pt₄₁Sn₂₄Ni₂₃Ga₁₂/C_{Plasma} are $2.62\text{ A g}_{\text{Pt}}^{-1}$, $1.28\text{ A g}_{\text{Pt}}^{-1}$ and $0.732\text{ A g}_{\text{Pt}}^{-1}$, respectively. This result indicates that Pt₄₅Sn₂₂Ni₂₁Ga₁₂/C_{XC72} and Pt₄₃Sn₂₄Ni₂₂Ga₁₁/C_{L6} electrocatalysts are much better than the Pt₄₁Sn₂₄Ni₂₃Ga₁₂/C_{Plasma} electrocatalyst. The quaternary Pt₄₅Sn₂₂Ni₂₁Ga₁₂/C_{XC72} ($1.27\text{ A g}_{\text{Pt}}^{-1}$) and Pt₄₃Sn₂₄Ni₂₂Ga₁₁/C_{L6} ($1.28\text{ A g}_{\text{Pt}}^{-1}$) electrocatalysts have higher current values with less Pt loading comparing to binary electrocatalysts, such as Pt₇₃Ir₂₇/C ($0.15\text{ A g}_{\text{Pt}}^{-1}$) [48], Pt₇₂Sn₂₈/C ($0.21\text{ A g}_{\text{Pt}}^{-1}$) [13], Pt₈₆Ni₁₅/C ($0.15\text{ A g}_{\text{Pt}}^{-1}$) [13]. The higher current values of the PtSnNiGa/C electrocatalysts might be related to the synergic effect of Sn, Ni and Ga.

The chronopotentiometric curves with the application of a current density of 3 mAcm^{-2} for 15 hours to quaternary PtSnNiGa/C electrocatalysts in 1.0 mol L⁻¹ ethanol solution in SE are shown in Figure 5B. The ethanol oxidation potential increases for all potentiometric curves in the early minutes of the experiment due to the poisoning of active sites by species, such as CO_{ads}, generated as ethanol oxidation occurs. After approximately 6 h

of the experiment, the electrocatalysts behave in different ways for the renewal of the active sites. The $\text{Pt}_{45}\text{Sn}_{22}\text{Ni}_{21}\text{Ga}_{12}/\text{C}_{\text{XC72}}$ and $\text{Pt}_{43}\text{Sn}_{24}\text{Ni}_{22}\text{Ga}_{11}/\text{C}_{\text{L6}}$ electrocatalysts show an increasing potential with time. $\text{Pt}_{41}\text{Sn}_{24}\text{Ni}_{23}\text{Ga}_{12}/\text{C}_{\text{Plasma}}$ electrocatalyst presents an oscillatory behaviour up to 12 h into the experiment. The oscillatory behaviour of potential curves vs time is commonly found in the oxidation of organic molecules, for example, methanol, ethanol and formic acid [51,52]. The oscillations might be associated with the presence of CO_{ads} from the alcohol oxidation. These oscillations prevent the electrode from being completely poisoned because the surface of the electrocatalyst is periodically renewed. The large amplitude fluctuations relate to a low electrocatalytic activity for CO_{ads} oxidation. Furthermore, the high potential achieved during the oscillations can cause degradation of the carbon support and degradation of the electrocatalyst. Low-frequency oscillations are the result of a low CO concentration in the electrode [51-53].

Figure 6 shows the cyclic voltammograms in the cycle 1, 500 and 1000. The EASA was estimated for the $\text{Pt}_{45}\text{Sn}_{22}\text{Ni}_{21}\text{Ga}_{12}/\text{C}_{\text{XC72}}$ and $\text{Pt}_{43}\text{Sn}_{24}\text{Ni}_{22}\text{Ga}_{11}/\text{C}_{\text{L6}}$ electrocatalysts after 1000 cycles in supporting electrolyte by integration of hydrogen desorption region $-0.15\text{ V} - 0.15\text{ V}$ vs $[\text{Ag}/\text{AgCl}, \text{KCl}_{\text{sat}}]$ subtracting the double layer contribution (see Table 3). After 1000 cycles the EASA values probably increases due to removal of surface blocking species. The metal concentration in SE solution, obtained with ICPE OES indicates that PtSnNiGa/C electrocatalysts are very stable regarding the metal loading once that metal concentration is about $\mu\text{g L}^{-1}$ (See Table S2 of [Supplementary Material](#)).

Table 3. EASA values for the PtSnNiGa electrocatalyst supported on Vulcan XC72 and Printex L6 carbons prepared by the DPP process*.

Electrocatalyst	EASA ₁ / m^2g^{-1}	EASA ₁₀₀₀ / m^2g^{-1}
$\text{Pt}_{45}\text{Sn}_{22}\text{Ni}_{21}\text{Ga}_{12}/\text{C}_{\text{XC72}}$	19.69	22.88
$\text{Pt}_{43}\text{Sn}_{24}\text{Ni}_{22}\text{Ga}_{11}/\text{C}_{\text{L6}}$	2.10	3.08

*It was not possible to calculate the EASA for the $\text{Pt}_{41}\text{Sn}_{24}\text{Ni}_{23}\text{Ga}_{12}/\text{C}_{\text{Plasma}}$ electrocatalyst because the cyclic voltammogram show no significant hydrogen desorption charge until 1000 cycles; EASA₁ = 1° CV cycle and EASA₁₀₀₀ = 1000° CV cycles.

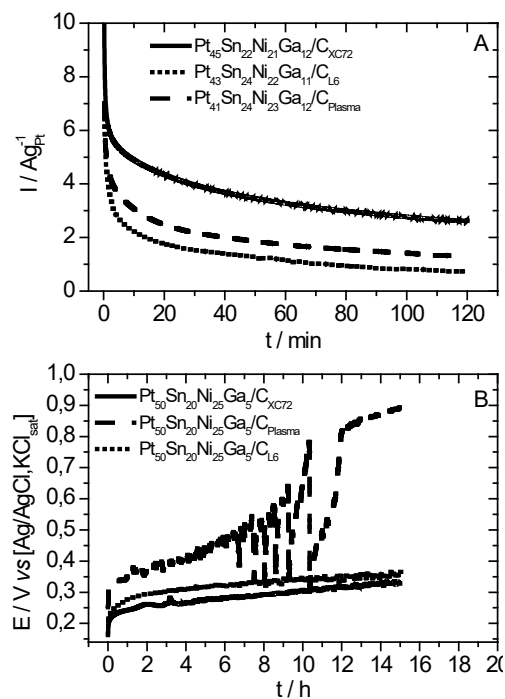


Figure 5: (A) CA at 0.2 V vs $[\text{Ag}/\text{AgCl}, \text{KCl}_{\text{sat}}]$ in ethanol 1.0 mol L^{-1} of PtSnNiGa/C electrocatalysts supported on Vulcan XC72, Printex-L6 and Black Plasma carbons. (B) CP at 3 mA cm^{-2} in ethanol 1.0 mol L^{-1} of PtSnNiGa/C electrocatalysts supported on Vulcan XC72, Printex-L6 and Black Plasma carbons.

The electrochemical impedance spectroscopy was carried out in ethanol 1.0 mol L^{-1} solution at 0.2 V vs $[\text{Ag}/\text{AgCl}, \text{KCl}_{\text{sat}}]$ in order to evaluating the electrical properties of $\text{Pt}_{45}\text{Sn}_{22}\text{Ni}_{21}\text{Ga}_{12}/\text{C}_{\text{XC72}}$, $\text{Pt}_{43}\text{Sn}_{24}\text{Ni}_{22}\text{Ga}_{11}/\text{C}_{\text{L6}}$, $\text{Pt}_{41}\text{Sn}_{24}\text{Ni}_{23}\text{Ga}_{12}/\text{C}_{\text{Plasma}}$ electrocatalysts for ethanol electrooxidation. The Nyquist (Figure 7A) and Bode (Figure 7B) plots shows that quaternary PtSnNiGa/C electrocatalysts have different behaviors regarding the EOR. The impedance arc size provides information about the charge transfer resistance (R_{ct}), long arcs indicates a slow rate for EOR. The equivalent circuit $[R_s(R_{\text{ct}}[QW])]$ (see Figure 8) consists of a solution resistance (R_s), a charge transfer resistance (R_{ct}), and constant phase element (Q) which are related to the capacitance of the double layer assuming the material roughness and a Warburg impedance (W), related to the diffusion process from the bulk of the solution to the electrode surface. It occurs that $\text{Pt}_{41}\text{Sn}_{24}\text{Ni}_{23}\text{Ga}_{12}/\text{C}_{\text{Plasma}}$ shows a high R_{ct} values (see Table 4) regarding $\text{Pt}_{45}\text{Sn}_{22}\text{Ni}_{21}\text{Ga}_{12}/\text{C}_{\text{XC72}}$ and $\text{Pt}_{43}\text{Sn}_{24}\text{Ni}_{22}\text{Ga}_{11}/\text{C}_{\text{L6}}$ electrocatalysts probably due to formation of intermediate species, such as CO_{ads} , strongly adsorbed on electrocatalyst active sites promoting the poisoning effect already known in the literature [54-59].

Table 4. Simulated [$R_s(R_{ct}[QW])$] circuit for the PtSnNiGa electrocatalyst supported on Vulcan XC72, Printex-L6

Circuit Element / unit	Electrocatalyst		
	Pt ₄₅ Sn ₂₂ Ni ₂₁ Ga ₁₂ /C _{XC72}	Pt ₄₃ Sn ₂₄ Ni ₂₂ Ga ₁₁ /C _{L6}	Pt ₄₁ Sn ₂₄ Ni ₂₃ Ga ₁₂ /C _{Plasma}
R_s / Ω	6.7	6.1	8.5
$W / \mu \Omega$	5.2	3.0	6.7
R_{ct} / Ω	245	246	390
Q / mF	10.4	15.6	1.56
N	0.94	0.96	0.86

* χ^2 observed for all simulations ranged from 10^{-2} to 10^{-3} and the error for simulated equivalent circuit parameters was obtained between 0.2 – 2.5%. Q is a constant phase element, R_s is the ohmic resistance, R_{ct} is charge transfer resistance and W is a Warburg impedance.

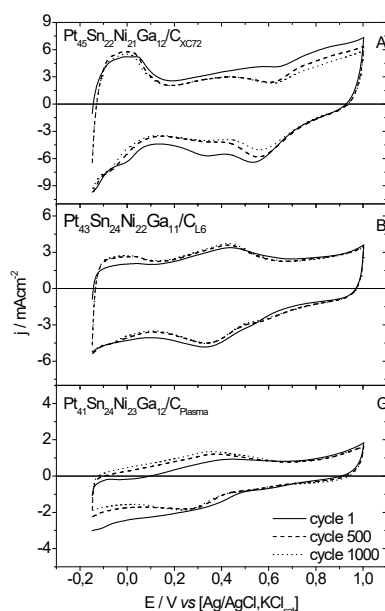


Figure 6. Stability test for (A) Pt₄₅Sn₂₂Ni₂₁Ga₁₂/C_{XC72} (B) Pt₄₃Sn₂₄Ni₂₂Ga₁₁/C_{L6} and (C) Pt₄₁Sn₂₄Ni₂₃Ga₁₂/C_{Plasma} in SE.

At low frequencies region, the deviations of phase angle, $-\phi$, from the ideal capacitor phase angle (90°) provides information about the pore size distribution. As can be seen in Figure 7B, the Pt₄₁Sn₂₄Ni₂₃Ga₁₂/C_{Plasma} electrocatalyst exhibit the largest phase angle deviation (58°) comparing to Pt₄₃Sn₂₄Ni₂₂Ga₁₁/C_{L6} (65°) and Pt₄₅Sn₂₂Ni₂₁Ga₁₂/C_{XC72} (61°) which indicates a larger pore size distribution. According Speder *et al.* [60], larger pores leads a nanoparticles aggregation that reduces electrochemical active surface as can be seen in TEM images. This behavior also can be seen for Pt₄₃Sn₂₄Ni₂₂Ga₁₁/C_{L6} despite of the phase angle. Therefore, the electrochemical impedance spectroscopy suggests that the Vulcan XC72 has appropriate pore size distribution for electrocatalysts nanoparticles dispersion.

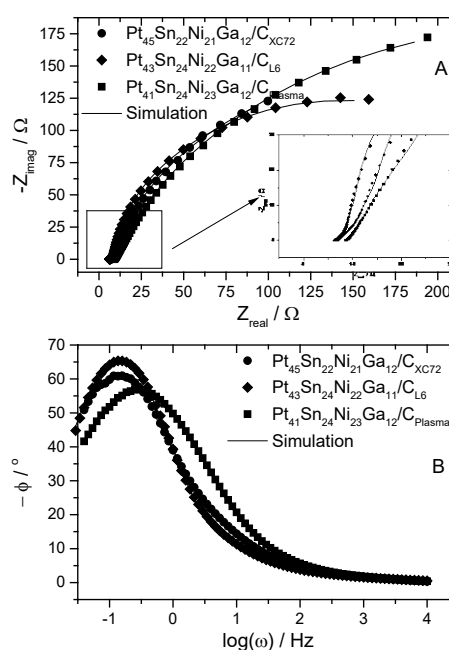


Figure 7. (A) Nyquist and (B) Bode plots of PtSnNiGa/C electrocatalysts.

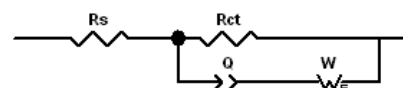


Figure 8. Simulated equivalent circuit for EOR in PtSnNiGa/C supported on Vulcan XC72, Printex-L6 and Black Plasma carbons.

4. CONCLUSION

In the present study, physicochemical and electrochemical investigations were performed to evaluate the influence of the carbon support on the catalytic activity of PtSnNiGa/C for the EOR. The Raman spectra indicates high graphitization of carbons supports which is related high electric conductivity. The EDS, TEM, and XRD data show that the electrocatalysts experimental composition are similar

and the estimated particle size are consistent with the sizes already reported in literature (2 nm – 7 nm) for Pt-based electrocatalysts. According to electrochemical analysis, the electrocatalyst supported on carbon Vulcan XC72 (Pt₄₅Sn₂₂Ni₂₁Ga₁₂/C_{XC72}) presents higher current normalized by Pt loading for ethanol electrooxidation, lower reactivity for CO poisoning process and lower charge transfer resistance comparing to the electrocatalysts supported on Printex-L6 and Plasma carbons, Pt₄₃Sn₂₄Ni₂₂Ga₁₁/C_{L6} and Pt₄₁Sn₂₄Ni₂₃Ga₁₂/C_{Plasma}, respectively. Results endorse that the carbon Vulcan XC72 is the better support regarding Printex L6 and Plasma mainly due to capability to the homogenous dispersion of electrocatalysts nanoparticles. Moreover, the reduced Pt loading quaternary electrocatalysts display better electrocatalytic activity towards EOR compared to high Pt loading electrocatalyst, such as Pt₇₂Sn₂₈/C, Pt₈₆Ni₁₅/C, Pt₇₃Ir₂₇/C and Pt₇₀Sn₂₅Ni₅/C, also showing that a small gallium addition has a promotional effect towards EOR.

5. ACKNOWLEDGMENTS

FAPES, CAPES, PETROBRAS, IFES and CNPq supported research described in this study.

6. REFERENCES AND NOTES

- [1] Chen, Z.; Higgins, D.; Yu, A.; Zhang L.; Zhang J. *Energy Environ. Sci.* **2011**, *4*, 3167. [\[CrossRef\]](#)
- [2] U.S. Department of Energy. Office of Fossil Energy. National Energy Technology Laboratory, Fuel Cell Handbook, EG&G Technical Services, 7th edition, 2004.
- [3] Brouzgou, A.; Song S. Q.; Tsiakaras, P. *Appl. Catal. B Environ.* **2012**, *127*, 371. [\[CrossRef\]](#)
- [4] Vigier, F.; Coutanceau, C.; Perrard, A.; Belgsir, E. M.; Lamy, C. *J. Appl. Electrochem.* **2004**, *34*, 439. [\[CrossRef\]](#)
- [5] Kamarudin, M. Z. F.; Kamarudin, S. K.; Masdar M. S.; Daud, W. R. W. *Int. J. Hydrogen Energy* **2013**, *38*, 9438. [\[CrossRef\]](#)
- [6] Figueiredo, M. C.; Sorsa, O.; Doan, N.; Pohjalainen, E.; Hildebrand, H.; Schmuki, P.; Wilson B. P.; Kallio, T. *J. Power Sources* **2015**, *275*, 341. [\[CrossRef\]](#)
- [7] Gupta, S. S.; Datta, J. *J. Electroanal. Chem.* **2006**, *594*, 65. [\[CrossRef\]](#)
- [8] Shao, M. H.; Adzic, R. R. *Electrochim. Acta* **2005**, *50*, 2415. [\[CrossRef\]](#)
- [9] Bonesi, A.; Triaca, W. E.; Castro Luna, A. M. *Port. Electrochim. Acta* **2009**, *27*, 193. [\[CrossRef\]](#)
- [10] Wang, Y.; Zou S.; Cai, W.-B. *Catalysts* **2015**, *5*, 1507. [\[CrossRef\]](#)
- [11] Li, H.; Sun, G.; Cao, L.; Jiang, L.; Xin, Q. *Electrochim. Acta* **2007**, *52*, 6622. [\[CrossRef\]](#)
- [12] Antolini E.; Gonzalez, E. R. *Catal. Today* **2011**, *160*, 28. [\[CrossRef\]](#)
- [13] Almeida, T. S.; Kokoh K. B.; De Andrade, A. R. *Int. J. Hydrogen Energy* **2011**, *36*, 3803. [\[CrossRef\]](#)
- [14] Bonesi, A. R.; Thomas J.; C. L. A. M. *LNLS Act. Rep. - Brazilian Synchrotron Light Lab.* **2009**, *5*.
- [15] Hogarth, M. P.; Ralph, T. R. *Platin. Met. Rev.* **2002**, *46*, 146. [\[CrossRef\]](#)
- [16] Kumar, V. B.; Sanetuntikul, J.; Ganesan, P.; Porat, Z.; Shanmugam S.; Gedanken, A. *Electrochim. Acta* **2015**, *190*, 659. [\[CrossRef\]](#)
- [17] Liu, Z.; Jackson G. S.; Eichhorn, B. W. *Energy Environ. Sci.* **2011**, *4*, 1900. [\[CrossRef\]](#)
- [18] Paganoto, G. T.; Santos, D. M.; Evangelista, T. C. S.; Guimarães, M. C. C.; Carneiro, M. T. W. D.; Ribeiro, J. *The Scientific World Journal*, **2017**, *2017*, 1. [\[CrossRef\]](#)
- [19] Tang, S.; Sun, G.; Qi, J.; Sun, S.; Guo, J.; Xin Q.; Haarberg, G. M. *Chinese J. Catal.* **2010**, *31*, 12. [\[CrossRef\]](#)
- [20] Sharma S.; Pollet, B. G. *J. Power Sources* **2012**, *208*, 96. [\[CrossRef\]](#)
- [21] Li, L.; Hu, L.; Li J.; Wei, Z. *Nano Res.* **2015**, *8*, 418. [\[CrossRef\]](#)
- [22] Wu, H.; Wexler D.; Liu, H. *Mater. Chem. Phys.* **2012**, *136*, 845. [\[CrossRef\]](#)
- [23] Zhao, X.; Li, W.; Jiang, L.; Zhou, W.; Xin, Q.; Yi B.; Sun, G. *Carbon N. Y.* **2004**, *42*, 3263.
- [24] Lee, K.; Zhang, J.; Wang H.; Wilkinson, D. P. *J. Appl. Electrochem.* **2006**, *36*, 507. [\[CrossRef\]](#)
- [25] Yoo, E.; Okata, T.; Akita, T.; Kohyama, M.; Nakamura J.; Honma, I. *Nano Lett.* **2009**, *9*, 2255. [\[CrossRef\]](#)
- [26] Evangelista, T. C. S.; Paganoto, G. T.; Guimarães, M. C. C.; Ribeiro, J. *J. Spectrosc.* **2015**, *2015*, 1. [\[CrossRef\]](#)
- [27] Assumpção, M. H. M. T.; De Souza, R. F. B.; Rascio, D. C.; Silva, J. C. M.; Calegari, M. L.; Gaubeur, I.; Paixão, T. R. L. C.; Hammer, P.; Lanza M. R. V.; Santos, M. C. *Carbon N. Y.* **2011**, *49*, 2842. [\[CrossRef\]](#)
- [28] Moraes, A.; Assumpção, M. H. M. T.; Simões, F. C.; Antonin, V. S.; Lanza, M. R. V.; Hammer, P.; Santos, M. C. *Electrocatalysis* **2016**, *7*, 60. [\[CrossRef\]](#)
- [29] Caliman, C. C.; Palma, L. M.; Ribeiro, J. *J. Electrochem. Soc.* **2013**, *160*, F853. [\[CrossRef\]](#)
- [30] Cunha, E. M.; Ribeiro, J.; K. Kokoh, B.; De Andrade, A. R. *Int. J. Hydrogen Energy* **2011**, *36*, 11034. [\[CrossRef\]](#)
- [31] Cullity, D.; Stock, S. R. *Elements of X Ray Diffraction.*, Prentice Hall Inc., Upper Saddle River, New Jersey, 3rd edn., 2001.
- [32] Escribano, R.; Sloan, J.J.; Siddique, N.; Sze, N.; Dudev, T. *Vib. Spectrosc.* **2001**, *26*, 179. [\[CrossRef\]](#)
- [33] Tuinstra, F.; Koenig, L. *J. Chem. Phys.* **1970**, *53*, 1126. [\[CrossRef\]](#)
- [34] Powder Diffraction File: 01-087-0646, vol. PDF-2, Joint Committee on Powder Diffraction Standards, International Center for Diffraction Data, Newtown Square, Pa, USA, 2011.
- [35] Callister, W. D.; Rethwisch, D. G. *Materials Science and Engineering: An Introduction*, Wiley, 8th edn., 2009.
- [36] D. P. Lide, *CRC Handbook of Chemistry and Physics*, Taylor & Francis, 89th edn., 2009.
- [37] Spinace, E. V L.; Vale, A. I.; Dias R. R.; Neto, A. O. *Carbon N. Y.* **2006**, *617*.

- [38] Spinacé, E. V.; Farias, L. A.; Linardi M.; Neto, A. O. *Mater. Lett.* **2008**, *62*, 2103. [[CrossRef](#)]
- [39] Perez, J.; Paganin V. A.; Antolini, E. J. *Electroanal. Chem.* **2011**, *654*, 108. [[CrossRef](#)]
- [40] Stevens D. A.; Dahn, J. R. *J. Electrochem. Soc.* **2003**, *150*, A770. [[CrossRef](#)]
- [41] Yadav, A. P. *Int. J. Chem. Stud.* **2013**, *1*, 189. [[CrossRef](#)]
- [42] Wang, H.; Jusys Z.; Behm, R. J. *J. Phys. Chem. B* **2004**, *108*, 19413. [[CrossRef](#)]
- [43] Climent, V.; Gómez, R.; Orts J. M.; Feliu, J. M. *J. Phys. Chem. B* **2006**, *110*, 11344. [[CrossRef](#)]
- [44] Ticianelli E. A.; González, E. R. *Eletroquímica*, Edusp, 2nd edn., 2013.
- [45] Dutta, A.; Mahapatra S. S.; Datta, J. *Int. J. Hydrogen Energy* **2011**, *36*, 14898. [[CrossRef](#)]
- [46] Leng, Y.; Wang X.; Hsing, I. J. *Electroanal. Chem.* **2002**, *528*, 145. [[CrossRef](#)]
- [47] Heinen, M.; Jusys Z.; Behm, R. J. *J. Phys. Chem. C* **2010**, *114*, 9850. [[CrossRef](#)]
- [48] Ribeiro, J.; dos Anjos, D. M.; K. Kokoh, B.; Coutanceau, C.; Léger, J. M.; Olivi, P.; de Andrade A. R.; Tremiliosi-Filho, G. *Electrochim. Acta* **2007**, *52*, 6997. [[CrossRef](#)]
- [49] Mayrhofer, K. J. J.; Arenz, M.; Blizanac, B. B.; Stamenkovic, V.; Ross P. N.; Markovic, N. M. *Electrochim. Acta* **2005**, *50*, 5144. [[CrossRef](#)]
- [50] Maillard, F.; Schreier, S.; Hanzlik, M.; Savinova, E. R.; Weinkauff S.; Stimming, U. *Phys. Chem. Chem. Phys.* **2005**, *7*, 385. [[CrossRef](#)]
- [51] Nagao, R.; Cantane, D. A.; Lima F. H. B.; Varela, H. J. *Phys. Chem. C* **2013**, *117*, 15098. [[CrossRef](#)]
- [52] Delmonde, M. V. F.; Nascimento, M. A.; Nagao, R.; Cantane, D. A.; Lima F. H. B.; Varela, H. J. *Phys. Chem. C* **2014**, *118*, 17699. [[CrossRef](#)]
- [53] Lopes, P. P.; Ticianelli E. A.; Varela, H. J. *Power Sources* **2011**, *196*, 84. [[CrossRef](#)]
- [54] Cericola D.; Spahr, M. E. *Electrochim. Acta* **2016**, *191*, 558. [[CrossRef](#)]
- [55] Orazem, M. E.; Tribollet, B. *Phys. Rev. (Series I)* **2008**, *14*, 533.
- [56] Kötz, R.; Carlen, M. *Electrochim. Acta* **2000**, *45*, 2483. [[CrossRef](#)]
- [57] Song, H.-K.; Jung, Y.-H.; Lee, K.; Lee, K.-H.; Dao, L. H. *Electrochim. Acta* **1999**, *44*, 3513. [[CrossRef](#)]
- [58] Song, H.-K.; Hwang, H.-Y.; Lee K.-H.; Dao, L. H. *Electrochim. Acta* **2000**, *45*, 2241. [[CrossRef](#)]
- [59] Musiani, M.; Orazem, M.; Tribollet B.; Vivier, V. *Electrochim. Acta* **2011**, *56*, 8014. [[CrossRef](#)]
- [60] Speder, J.; Zana, A.; Spanos, I.; Kirkensgaard, J. J. K.; Mortensen, K.; Hanzlik, M.; Arenz, M. *J. Power Sources* **2014**, *261*, 8. [[CrossRef](#)]